

Torsional deformation of an endoscope probe

BY FOTINI V. KATOPODES¹, J. R. BARBER² AND YANSONG SHAN³

¹*Department of Civil and Environmental Engineering,
Stanford University, Stanford, CA 94305, USA*

²*Department of Mechanical Engineering, University of Michigan,
Ann Arbor, MI 48109-2125, USA*

³*General Robotic Devices Inc., 40 Clark Street, Suite C,
Salinas, CA 939017, USA*

Received 4 October 2000; accepted 9 April 2001

A recent US patent due to Shan describes a method for identifying the location of the colonoscope in the body during endoscopy. The method depends upon the integration of measurements recorded by a flexible probe inserted in the biopsy channel at the end of a flexible rod.

In this paper, classical results for the elastic rod are used to determine the equations required for this integration process. Particular attention is paid to the effect of initial curvature or non-axisymmetry of the rod. It is shown that these effects cause predictive errors that increase quadratically with the angle subtended by the space curve of the channel, and quite stringent limits must be placed on straightness and symmetry if these errors are not to be significant.

Keywords: colonoscopy; endoscope; elastic rod; form errors

1. Introduction

Cancer of the colon and rectum ranks second only to lung cancer as the most common form of cancer and is the leading cause of cancer mortality in the United States. Colon cancer often develops from small non-cancerous growths in the colon called polyps. Studies have shown that by undergoing a colonoscopy examination and having polyps removed, a significant reduction in colon cancer mortality could be achieved (Hellinger 1998). During colonoscopy, a flexible fibre-optic scope (endoscope, colonoscope) is inserted through the anus, permitting the interior of the entire length of the colon to be visualized on a television monitor. The patient is sedated during the procedure.

The benefits of colonoscopy must be weighed against the discomfort of the procedure and the potential for serious complications, such as colonic perforation. Problems arise because of the high degree of variability in the anatomy of the colon from person to person, the possibility of looping or kinking of the flexible scope, and the difficulty in determining the position of the tip of the scope. Colonoscopy may be combined with simultaneous radiological screening to produce an image of a small part of the instrument (Rogers 1990), but has several disadvantages: of increasing the cost of the procedure, exposing the patient and possibly the staff to X-rays, requiring protective screening, and having access to X-ray equipment at the outpatient examination site.

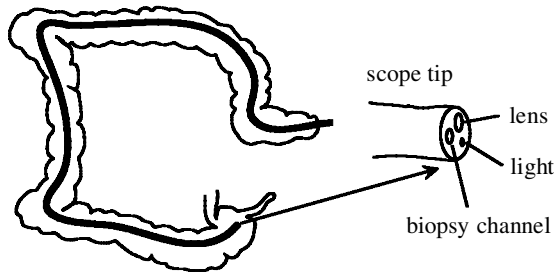


Figure 1. Insertion of the endoscope in the colon (left) and detailed cross-section of the endoscope (right).

Several authors have proposed non-radiological methods for the three-dimensional imaging of the endoscope. Williams *et al.* (1993) located a set of coils along the endoscope which respond to low-power electrical currents passed through a wire grid placed under the mattress on the examination surface. A similar method due to Bladen *et al.* (1993) uses an inductive sensor responding to a low-strength magnetic field produced by three discrete generators in different orientations.

(a) *Shan's endoscope*

In a recent US patent, Shan (1999) describes a new method that does not rely on the presence of external radiation or magnetic fields. The endoscope is first inserted into the colon, as shown in figure 1. The scope contains a 'biopsy channel' through which surgical instruments may be inserted and controlled for the removal of polyps or biopsy samples. In Shan's method, the location of the endoscope tip is determined by using a flexible rod to push a flexible probe down the biopsy channel. The probe is instrumented with strain gauges, the output of which provides information as to the local curvature of the channel in two dimensions. An encoder at the inlet to the channel records the velocity and distance of the probe as it is pushed through the channel. Integration of the curvature information enables the three-dimensional space curve defining the channel to be constructed and displayed graphically. The advantages of this technique are that it obviates the need for equipment above or surrounding the abdomen of the patient and it has no radiation risks. Notice that the measurements are made after the endoscope has been inserted and that the probe is inserted through the accurately manufactured biopsy channel rather than directly into the colon itself. Thus, it should be possible to control measurement accuracy, provided the forces required for insertion are not sufficient to cause motion of the endoscope during measurement.

In order to interpret the strain gauge data, we need to know the rotational orientation of the probe at each stage in the insertion process. This can be determined from the condition that there be no torque on the free end of the rod, using Love's (1927) theory of thin rods. Experiments were performed to validate the concept and showed generally good predictions of position under a variety of endoscope configurations, except that erratic predictions were obtained for a subset of the rods used. These errors were eventually traced to the presence of small but measurable amounts of curvature in the unloaded state of the offending rods. If a rod with initial curvature is bent further until it forms a plane circle of radius R , the strain energy in this state will be smaller than that if the rod is bent *against* its initial curvature into

a circle of the same radius. This will tend to make the initially curved rod twist to follow the direction in the channel that minimizes total strain energy, and if the initial curvature is not allowed for in the integration process, it will lead to errors of data interpretation. Related effects can be produced if the rod is initially straight but is slightly out of round, so that the principal second moments of area (flexural rigidities) are unequal.

(b) *Scope of this paper*

In this paper, we shall develop the equations permitting the position of the probe to be determined from the sequence of curvature measurements for both perfect and imperfect rods. In particular, we shall investigate the effect of small imperfections on the resulting trajectory with a view to defining the level of tolerances on straightness and out of roundness that must be achieved if the method is to be viable. We shall also show that snap-through instabilities can occur if the initial imperfection and the subtended angle of the channel are sufficiently large.

The equations governing the equilibrium of an elastic rod are conveniently summarized by Love (1927), whose notation we shall generally follow in the present paper. Numerous other formulations have since been derived that are particularly suited to specific problems for the rod. For example, Nordgren (1974) presents a vector formulation for the motion of a rod with equal flexural rigidities, while Lu & Perkins (1994) use Hamilton's principle to develop a stability analysis of large deformation equilibria of a rod loaded only by end forces and couples. A comprehensive review of rod theories is given by Antman (1974).

2. Kinematics

The probe is inserted in a precisely manufactured lubricated channel in the endoscope, so friction should be negligible. This is confirmed by the experimental observation that the axial force required during insertion is negligible. It follows that the axial strain of the rod will be zero at all points. Hence, if the coordinate $s(t)$ records the length of rod that has been pushed into the channel at time t , the free end will be located at a distance s along the centreline of the channel.

Following Love (1927, § 253), we identify a fixed Cartesian axis system x, y, z and a moving axis system x', y', z' . The moving axis system is such that z' is aligned with the local tangent to the centreline of the rod and increases with s , while the orthogonal axes x', y' correspond to lines passing through a generator of the rod in the undeformed state. If the rod has differing values of principal second moment of area, x', y' can be chosen to follow these axes along the rod. In the special case where $I_1 = I_2$, we can conveniently choose to identify x', y' with the axes at which the sensors are located on the end of the rod.

The angles between the system x', y', z' and x, y, z can be defined in terms of direction cosines, following Love (1927, § 253, eqn (4)), or in terms of rotation angles θ, ψ, ϕ defined in fig. 46 of Love (1927). In particular, we note that

$$\frac{dx}{ds} = \frac{\partial x}{\partial z'} = l_3, \quad \frac{dy}{ds} = \frac{\partial y}{\partial z'} = m_3, \quad \frac{dz}{ds} = \frac{\partial z}{\partial z'} = n_3, \quad (2.1)$$

where the direction cosines l_3, m_3, n_3 are given by Love (1927, § 253, eqn (7)) as

$$l_3 = \sin \theta \cos \psi, \quad m_3 = \sin \theta \sin \psi, \quad n_3 = \cos \theta. \quad (2.2)$$

The centreline of the rod is completely characterized by the two angles $\theta(s)$, $\psi(s)$. If these angles were known for all s , we would be able to integrate equations (2.1) with respect to s and hence determine the coordinates $x(s)$, $y(s)$, $z(s)$ of all points on the rod.

The curvatures and twist of the rod at any given point are denoted by κ , κ' , τ . They are defined as the rate of rotation of the axis system x', y', z' as we progress along the curve in the direction of positive s , resolved into components in the directions x' , y' , z' , respectively. Thus, τ represents the rate of rotation about the z' axis and hence represents twist per unit length, while κ , κ' represent bending curvatures about orthogonal axes fixed with respect to the undeformed rod. These quantities are related to the rotation angles θ , ψ , ϕ by the equations

$$\kappa = \frac{d\theta}{ds} \sin \phi - \frac{d\psi}{ds} \sin \theta \cos \phi, \quad \kappa' = \frac{d\theta}{ds} \cos \phi + \frac{d\psi}{ds} \sin \theta \sin \phi, \quad (2.3)$$

$$\tau = \frac{d\phi}{ds} + \frac{d\psi}{ds} \cos \theta, \quad (2.4)$$

from Love (1927, § 253, eqns (8)). With a suitable choice of convention for x' , y' , κ , κ' could represent the calibrated signals for rod curvature. With a more general choice of coordinates, they will simply be these quantities rotated through some constant angle.

3. Equilibrium

We next note that the forces in the rod must satisfy six differential equations of equilibrium, which are eqns (10) and (11) of § 254 of Love (1927). Only one of these equations will concern us here, this being the equation of moment equilibrium about the z' -axis. The channel is assumed to be frictionless, so there can be no external moment about this axis on an infinitesimal segment. Thus, the quantity Θ in the third of Love's eqns (11) must be zero and we have

$$\frac{dT}{ds} - M\kappa' + M'\kappa = 0, \quad (3.1)$$

where T is the torque and M , M' are the moments about the axes x' , y' , respectively.

If the rod has principal second moments of area I_1 , I_2 , respectively, we have

$$M = EI_1(\kappa - \kappa_0), \quad M' = EI_2(\kappa' - \kappa'_0), \quad (3.2)$$

where E is Young's modulus and $\kappa_0(s)$, $\kappa'_0(s)$ describe the initial curvature of the rod. Substituting these results in equation (3.1), we obtain

$$\frac{dT}{ds} = EI_1\kappa'(\kappa - \kappa_0) - EI_2\kappa(\kappa' - \kappa'_0). \quad (3.3)$$

4. Insertion of the rod in a specified channel

Suppose now that we take a rod with known initial curvature and insert it into a channel of known shape. Thus, $\kappa_0(s)$, $\kappa'_0(s)$ and $\theta(s)$, $\psi(s)$ will be known functions of s , but $\phi(s)$ is unknown and remains to be found from equation (3.3) with suitable end conditions. Substituting (2.3) into (3.3), we obtain

$$\frac{dT}{ds} = f_1(s) \cos \phi + f_2(s) \sin \phi + f_3(s) \cos(2\phi) + f_4(s) \sin(2\phi), \quad (4.1)$$

where f_1, f_2, f_3, f_4 are known functions of s given by

$$f_1 = -EI_1\kappa_0 \frac{d\theta}{ds} - EI_2\kappa'_0 \frac{d\psi}{ds} \sin \theta, \quad f_2 = EI_2\kappa'_0 \frac{d\theta}{ds} - EI_1\kappa_0 \frac{d\psi}{ds} \sin \theta, \quad (4.2)$$

$$f_3 = -E(I_1 - I_2) \frac{d\theta}{ds} \frac{d\psi}{ds} \sin \theta, \quad f_4 = \frac{E(I_1 - I_2)}{2} \left[\left(\frac{d\theta}{ds} \right)^2 - \left(\frac{d\psi}{ds} \sin \theta \right)^2 \right]. \quad (4.3)$$

To complete the solution for $\phi(s)$, we note that

$$T(s) = GK\tau(s), \quad (4.4)$$

where GK is the torsional rigidity of the rod and τ is given by equation (2.4). Hence,

$$\frac{dT}{ds} = GK \left(\frac{d^2\phi}{ds^2} + f_5(s) \right), \quad (4.5)$$

where

$$f_5 = \frac{d}{ds} \left(\frac{d\psi}{ds} \cos \theta \right) = \frac{d^2\psi}{ds^2} \cos \theta - \frac{d\psi}{ds} \frac{d\theta}{ds} \sin \theta \quad (4.6)$$

is another known function of s . Finally, equating (4.1) and (4.5) and rearranging terms, we have

$$\frac{d^2\phi}{ds^2} = \frac{1}{GK} [f_1(s) \cos \phi + f_2(s) \sin \phi + f_3(s) \cos(2\phi) + f_4(s) \sin(2\phi)] - f_5(s), \quad (4.7)$$

which is an ordinary differential equation for ϕ .

(a) End conditions

The rod is fed into the channel at a known orientation ϕ_0 and the other end of the rod ($s = s_1$) is free of torque. The end conditions are therefore

$$\phi(0) = \phi_0, \quad T(s_1) = 0. \quad (4.8)$$

The second of these conditions implies that

$$\frac{d\phi}{ds} = -\frac{d\psi}{ds} \cos \theta, \quad s = s_1, \quad (4.9)$$

from equations (4.4) and (2.4).

The numerical solution of equation (4.7) is slightly complicated by the fact that the two boundary conditions (4.8) and (4.9) are specified at opposite ends of the rod. An appropriate numerical strategy is to guess the value $\phi(s_1) \equiv \phi_1$ and use this and (4.9) as initial conditions for an integration from $s = s_1$ to $s = 0$ to obtain the corresponding value of ϕ_0 . Iteration on ϕ_1 will then enable the solution for specified ϕ_0 to be obtained.

5. The inverse solution

Next we consider the inverse problem in which the space curve is *unknown* and measurements of κ, κ' are to be used to determine it and, in particular, to determine the coordinates x, y, z of the end of the endoscope after insertion.

(a) *Initially straight axisymmetric rod*

We first consider the special case in which the rod is initially straight and axisymmetric, so that $\kappa_0 = \kappa'_0 = 0$ and $I_1 = I_2$. In this case, the four functions f_1, f_2, f_3, f_4 are zero from equations (4.2), (4.3), and it follows from (4.1) and the second of (4.8) that the torque T , and hence also the twist τ , are zero for all s . Equation (2.4) then reduces to

$$\frac{d\phi}{ds} + \frac{d\psi}{ds} \cos \theta = 0, \quad (5.1)$$

and we can solve equations (2.3), (5.1) for the three derivatives to obtain

$$\frac{d\theta}{ds} = \kappa \sin \phi + \kappa' \cos \phi, \quad (5.2)$$

$$\frac{d\psi}{ds} = \frac{\kappa' \sin \phi - \kappa \cos \phi}{\sin \theta}, \quad (5.3)$$

$$\frac{d\phi}{ds} = \frac{\kappa \cos \phi - \kappa' \sin \phi}{\tan \theta}. \quad (5.4)$$

Now suppose that the coordinates x, y, z and the angles θ, ψ, ϕ are known at some point s . We have experimental data for κ, κ' at s , so we can use equations (5.2)–(5.4) to determine the local values of the three derivatives. The three angles at $s + \delta s$ can then be updated according to

$$\theta(s + \delta s) = \theta(s) + \delta s \frac{d\theta}{ds}(s) \quad (5.5)$$

and two similar equations. We can also update the position coordinates x, y, z in the same way, using equations (2.1), (2.2).

Experimental tests of this methodology were performed using various circular and helical configurations for the endoscope. Generally good results were obtained with the spatial location of the probe being predicted to within a few millimetres, except for a few cases in which the rods were found to have small but measurable amounts of curvature in the unloaded state. The effect of such initial imperfections will be investigated in the following sections.

(b) *Initially curved or non-axisymmetric rod*

The inverse problem is considerably more complex when the rod has initial curvature or is not axisymmetric, since the value of ϕ at a given point in the channel will then generally vary during insertion. To understand why this is so, note that as we push the rod further in,

- (i) specific points on the rod are located at new points in the channel, changing the right-hand side of (4.7), and
- (ii) the segment of rod $0 < s < s_1$ is free of torque at $s = s_1$ when insertion has proceeded only to that point, but is subjected to a torque at $s = s_1$ when insertion has proceeded as far as $s = s_2 (> s_1)$.

This torque influences the twist τ throughout the length of the rod and hence affects ϕ everywhere, even in the special case where κ_0, κ'_0 are constant along the rod. By

contrast, when the rod is initially straight and axisymmetric, we have seen that the torque is everywhere zero, so the value of ϕ in $0 < s < s_1$ would not be changed if we were to remove the segment of rod between s_1 and the free end s_2 .

We can solve the inverse problem in the more general case using an updating algorithm. We assume provisionally that the space curve is known up to some point s_1 , i.e. $\theta(s)$, $\psi(s)$ are known in $0 < s < s_1$. We can therefore use the algorithm of §4 to determine ϕ_1 , defined as the value of ϕ at the free end of the rod when it is pushed in just to the point $s = s_1$. At this point, the probe measures the values κ_1 , κ'_1 at $s = s_1$ and equations (2.3) permit us to solve for the derivatives of θ , ψ as

$$\frac{d\theta}{ds}(s_1) = \kappa_1 \sin \phi_1 + \kappa'_1 \cos \phi_1, \quad (5.6)$$

$$\frac{d\psi}{ds}(s_1) = \frac{\kappa'_1 \sin \phi_1 - \kappa_1 \cos \phi_1}{\sin \theta_1}, \quad (5.7)$$

where $\theta_1 \equiv \theta(s_1)$. We can therefore find the updated values of θ , ψ using

$$\theta(s_1 + \delta s) = \theta(s_1) + \delta s \frac{d\theta}{ds}(s_1), \quad \psi(s_1 + \delta s) = \psi(s_1) + \delta s \frac{d\psi}{ds}(s_1). \quad (5.8)$$

The probe is then pushed in to the next measurement point and the process is repeated.

6. The circular channel

We would not deliberately manufacture a rod that is initially curved or non-axisymmetric. The principal purpose of the more general analysis above is to enable us to assess the degree of manufacturing error that can be tolerated if the simpler predictive algorithm of §5*a* is to give acceptable accuracy. For this purpose we consider the special case in which an imperfect rod is inserted into a channel defined by a plane circle.

We choose the fixed coordinate system so that the circle of radius R_1 lies in the xz -plane, as shown in figure 2. Elementary calculations then show that $\psi = 0$ everywhere and that θ is equal to the angle subtended at the centre of the circle. We also have $s = R_1\theta$ and hence

$$\frac{d\theta}{ds} = \frac{1}{R_1} \equiv \rho_1, \quad (6.1)$$

where ρ_1 is the curvature of the channel. It then follows from equations (2.3) that

$$\kappa = \rho_1 \sin \phi, \quad \kappa' = \rho_1 \cos \phi. \quad (6.2)$$

We also have $f_5 = 0$ from equation (4.6).

(a) Axisymmetric rod with constant curvature

Suppose that the rod has equal principal second moments of area $I_1 = I_2 \equiv I$ and a constant initial curvature ρ_0 . There are no principal axes in this case, so we can arbitrarily choose the rod coordinate system to align the initial curvature with the y -axis, giving

$$\kappa_0 = 0, \quad \kappa'_0 = \rho_0. \quad (6.3)$$

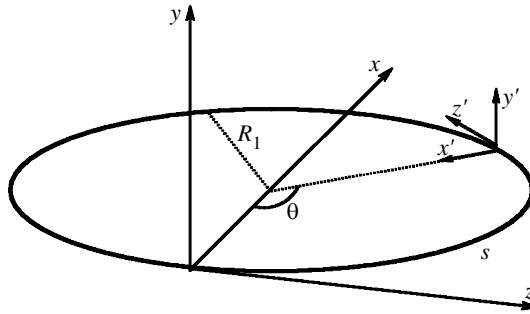


Figure 2. The plane circular channel.

Substituting these results into (4.2), (4.3), we find that the only non-zero function is

$$f_2 = EI\rho_0\rho_1, \quad (6.4)$$

and hence equation (4.7) reduces to

$$\frac{d^2\phi}{ds^2} = \frac{EI}{GK}\rho_0\rho_1 \sin\phi. \quad (6.5)$$

Alternatively, equation (6.5) can be written in terms of the subtended angle θ as

$$\frac{d^2\phi}{d\theta^2} = \Lambda \sin\phi, \quad (6.6)$$

where

$$\Lambda = \frac{EI}{GK} \frac{\rho_0}{\rho_1}. \quad (6.7)$$

The end conditions are

$$\phi(0) = \phi_0, \quad \frac{d\phi}{d\theta}(\theta_1) = 0, \quad (6.8)$$

from (4.8), (4.9), (6.1).

Notice, incidentally, that equation (6.6) is identical to that describing the motion of a pendulum when the displacements cannot be assumed to be small, the angle ϕ being measured from the unstable upper equilibrium position and θ playing the role of time.

A formal analytical solution can be obtained by writing

$$\frac{d\phi}{d\theta} = \varphi, \quad \frac{d^2\phi}{d\theta^2} = \frac{d\varphi}{d\theta} = \varphi \frac{d\varphi}{d\phi}. \quad (6.9)$$

Equation (6.6) then takes the form

$$\varphi \frac{d\varphi}{d\phi} = \Lambda \sin\phi, \quad (6.10)$$

and separation of variables followed by integration yields the solution

$$\varphi^2 = -2\Lambda \cos(\phi) + C, \quad (6.11)$$

where C is a constant.

The constant C can be expressed in terms of the unknown end rotation $\phi_1 \equiv \phi(\theta_1)$ using the second of (6.8) and (6.9), with the result

$$\varphi^2 = 2\Lambda[\cos(\phi_1) - \cos(\phi)]. \quad (6.12)$$

We can then substitute for φ from (6.9) and separate variables again, to obtain

$$\theta = - \int_{\phi_0}^{\phi} \frac{d\phi}{\sqrt{2\Lambda[\cos(\phi_1) - \cos(\phi)]}}. \quad (6.13)$$

Notice that we have selected the negative root of (6.12) because we anticipate that the rod will relax from ϕ_0 towards the minimum energy orientation $\phi = 0$ with increasing θ as long as $0 < \phi_0 < \pi$. Different conventions are required in other ranges. For example, in $\pi < \phi_0 < 2\pi$, relaxation will occur towards the state $\phi = 2\pi$ and the positive root should be taken.

Equation (6.13) is not a very convenient form, because the integral is an incomplete elliptic integral and it is not easy to impose the second end condition. Also, it implicitly assumes that ϕ is a single-valued function of θ and hence varies monotonically with θ . This condition is satisfied for sufficiently small values of Λ , but at larger values we find oscillations which invalidate the integration process. However, there is no difficulty in obtaining results numerically for specified combinations of ϕ_0 , Λ , and we shall do this in § 6c below.

(b) Conditions for minimal end rotation

The object of the investigation is to define appropriate criteria to determine when the initial curvature ρ_0 is sufficiently small for the probe position to be regarded as known. Under these satisfactory operating conditions, ϕ differs only slightly from ϕ_0 and ϕ_1 and hence we can solve equation (6.6) using an asymptotic method.

We first define a small deviation function ϵ through the equation

$$\phi = \phi_1 + \epsilon, \quad (6.14)$$

in which case

$$\cos(\phi) \approx (\cos(\phi_1) - \epsilon \sin(\phi_1)). \quad (6.15)$$

Substituting into (6.13) and integrating, we obtain

$$2(\epsilon_0^{1/2} - \epsilon^{1/2}) = \theta \sqrt{2\Lambda \sin(\phi_1)}, \quad (6.16)$$

where $\epsilon_0 = \phi_0 - \phi_1$ is the relative rotation between the two ends of the rod.

Since $\epsilon \ll 1$, there is little approximation involved in replacing ϕ_1 by ϕ_0 in equation (6.16). The definition (6.14) shows that $\epsilon = 0$ when $\theta = \theta_1$ and hence

$$\epsilon_0 = \frac{1}{2}\theta_1^2 \Lambda \sin(\phi_0). \quad (6.17)$$

The maximum value of this error is obtained when $\phi_0 = \pi/2$ and is

$$\epsilon_0^{\max} = \frac{1}{2}\theta_1^2 \Lambda = \frac{\theta_1^2 EI}{2GK} \frac{\rho_0}{\rho_1}, \quad (6.18)$$

from (6.7). For an axisymmetric section, $K = 2I$ and, hence, using $E = 2(1 + \nu)G$, we have

$$\frac{EI}{GK} = (1 + \nu) \quad (6.19)$$

and

$$\epsilon_0^{\max} = \frac{\theta_1^2(1 + \nu)}{2} \frac{\rho_0}{\rho_1}. \quad (6.20)$$

Notice that the error increases quadratically with θ_1 . For a channel defining one complete circle ($\theta_1 = 2\pi$) and a maximum error of $\epsilon_0^{\max} = 0.01$ rad we must have

$$\frac{\rho_0}{\rho_1} < 4 \times 10^{-4}, \quad (6.21)$$

for Poisson's ratio $\nu = 0.3$. This places quite strict requirements on the initial straightness of the rod. For example, if the channel describes a circle of radius 100 mm ($\rho_1 = 0.01 \text{ mm}^{-1}$), the rod must not deviate from the straight by more than 1 mm at the centre of a 600 mm length. For this reason, it is clearly essential that great care be taken to ensure that the rod does not get deformed as a result of misuse. In particular, it should be stored in a stiff housing from which it is directly inserted into the channel.

Equation (6.20) can be rewritten

$$\epsilon_0^{\max} = \frac{(1 + \nu)R_1\theta_1^2}{2R_0} = \frac{(1 + \nu)s_1\theta_1}{2R_0}, \quad (6.22)$$

where $s_1 = R_1\theta_1$ is the arc length of the segment and θ_1 is the subtended angle. In other words, the maximum error in the predicted orientation ϕ_1 of the probe is proportional to the product of the subtended angle of the trajectory θ_1 and the inserted length of the rod s_1 . It is reasonable to assume that a similar qualitative dependence on these parameters would apply to the more complex channel configurations found in the colon, since these can be considered as a concatenation of circular segments of various radii and orientations.

(c) Numerical results

For larger values of Λ , the relation between ϕ_0 and ϕ_1 is easily obtained by numerical integration. As suggested in § 4a above, the most convenient approach is to take ϕ_1 as given, in which case two boundary conditions are defined at $\theta = \theta_1$. We can then integrate equation (6.6) numerically from θ_1 to zero to find the corresponding value of ϕ_0 .

Results for various values of Λ are presented in figure 3. These results can be generalized to arbitrary θ_1 by replacing Λ by Λ^* defined by

$$\Lambda^* = \frac{EI}{GK} \left(\frac{\theta_1}{2\pi} \right)^2 \frac{\rho_0}{\rho_1}. \quad (6.23)$$

For very small Λ , the results show a small sinusoidal deviation from the line $\phi_1 = \phi_0$, as predicted by equation (6.17). For $\Lambda = 0.02$, the asymptotic analysis predicts a maximum deviation of $\epsilon_0^{\max} = 22.6^\circ$. This compares with a numerical value of 22.0° (not shown in figure 3), showing that the asymptotic analysis gives a good approximation up to this value of Λ .

Some insight into the results for larger values of Λ can be gained by recalling that equation (6.6) also describes the motion of a pendulum, where ϕ is the angle between the pendulum and the unstable vertically upwards equilibrium position,

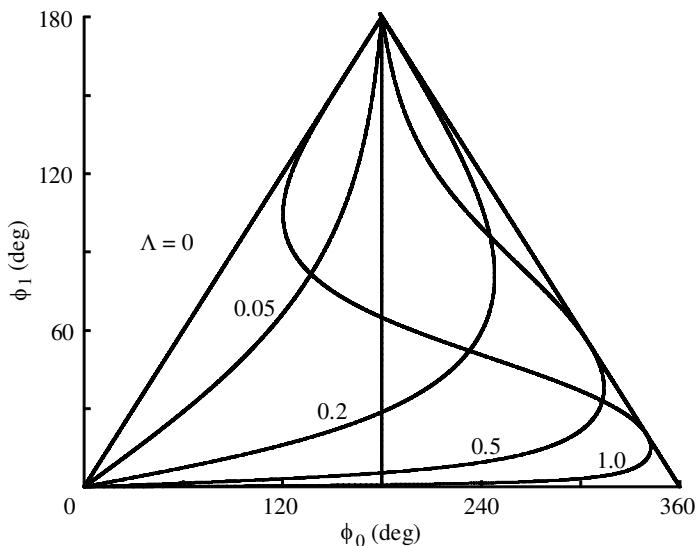


Figure 3. Relation between ϕ_1 and ϕ_0 for various values of Λ .

and θ represents time. Since $d\phi/d\theta = 0$ at $\phi = \phi_1$, the analogous dynamical problem concerns the pendulum released from rest at the position $\phi = \phi_1$.

When $\Lambda^* \ll 1$, only a small amount of motion occurs during the ‘time’ $0 < \theta < \theta_1$, and hence $\phi_0 - \phi_1 \ll 1$. As Λ^* is increased, the amplitude of motion in this period increases until eventually the range $0 < \theta < \theta_1$ captures an entire half period, with ϕ reaching $2\pi - \phi_1$. Further increase in Λ^* will lead to solutions in which ϕ is a non-monotonic function of θ . For given Λ^* , the period $\bar{\theta}$ of the pendulum tends to a minimum value

$$\bar{\theta}^* = \frac{2\pi}{\sqrt{\Lambda^*}}, \tag{6.24}$$

when the amplitude of oscillations is small. This occurs when the pendulum is released from a point near the lower stable equilibrium configuration, and hence non-monotonicity will occur first when ϕ_1 is close to π .

We know from energy arguments that the pendulum cannot escape the region $\phi_1 < \phi < 2\pi - \phi_1$, and this is clearly demonstrated in the results in figure 3. The solution will be monotonic for all ϕ_1 as long as the length θ_1 is less than the half period $\bar{\theta}^*/2$, and hence

$$\Lambda^* = \Lambda \left(\frac{\theta_1}{2\pi} \right)^2 < \Lambda \left(\frac{\bar{\theta}^*}{4\pi} \right)^2 = \frac{1}{4}, \tag{6.25}$$

using (6.24). Also, if θ_1 is less than a *quarter* period ($\Lambda^* < \frac{1}{16}$), ϕ_0 and ϕ_1 must both lie on the same side of $\phi = \pi$, and hence the entire curve in figure 3 lies to the left of the line $\phi_0 = \pi$. These conclusions are all confirmed by the curves in figure 3.

For $\Lambda^* > \frac{1}{4}$, the curves cross the line $\phi_0 = \pi$ a second time near the point (π, π) . More generally, the number of crossings of this line in the range $0 < \phi_1 < \pi$ will be the integer part of $4\sqrt{\Lambda^*}$, corresponding to the number of half periods in $0 < \theta < \theta_1$.

The results of figure 3 can be extended into other ranges by symmetry arguments, as illustrated in figure 4 for $\Lambda^* = 0.05, 0.2$. We conclude that ϕ_1 is a monotonic

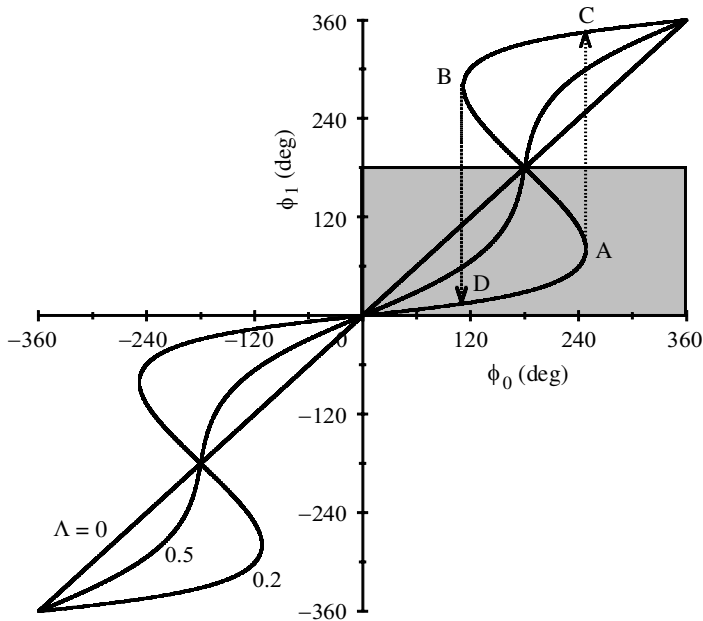


Figure 4. Extension of figure 2 using symmetry arguments. The shaded area represents that part of the response plotted in figure 2.

single-valued function of ϕ_0 for $\Lambda^* < \frac{1}{16}$, but above this limiting value there are multi-valued regions. Such regions will be unstable in the sense that increasing ϕ_0 monotonically will lead to a ‘snap through’ from A to C in figure 4 with increasing ϕ_0 . A similar snap through from B to D will occur with decreasing ϕ_0 . The solutions between A and B are inaccessible using any (not necessarily monotonic) input history $\phi_0(t)$. For the same reason, the more complex oscillations in the curve obtained near (π, π) for large Λ^* are also inaccessible and of only academic interest.

7. Torque variation

Snap-through instabilities can occur below the threshold established in the previous section if the rod is pushed into the channel by a torsionally flexible drive. To investigate this effect, we consider the problem in which the initially curved rod of § 6 is first fully inserted in the plane circular channel and then rotated by the application of a torque T_0 at the fixed end $\theta = \theta_0$. The torque at any section is given by equation (4.4), so using (2.4), (6.1), (6.9), (6.12) and setting $\phi = \phi_0$, we obtain

$$T_0 = \pm GK \rho_1 \sqrt{2\Lambda^* [\cos(\phi_1) - \cos(\phi_0)]}. \tag{7.1}$$

A convenient dimensionless measure of this torque can be defined as

$$T^* \equiv \frac{T_0}{GK \sqrt{(1 + \nu)\rho_0\rho_1}} = \pm \sqrt{2[\cos(\phi_1) - \cos(\phi_0)]} \tag{7.2}$$

using (6.7), (6.19). The sign of the square root in these expressions is most easily determined by reference to the pendulum analogy of § 6. For small values of Λ^* , we take the negative root for $0 < \phi_0 < \pi$ and the positive root for $\pi < \phi_0 < 2\pi$.

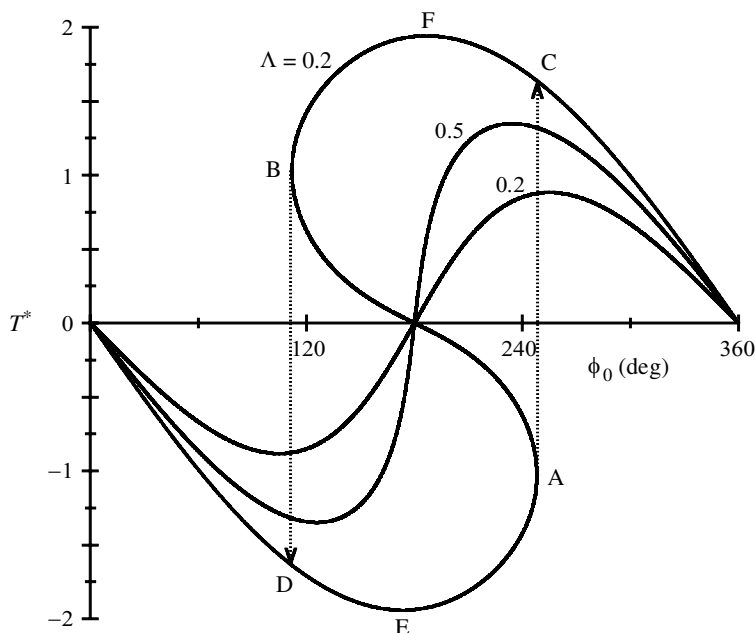


Figure 5. Relation between input torque and input angle (in degrees).

The dimensionless torque is plotted in figure 5 for various values of Λ^* . For $\Lambda^* \ll 1$, T^* is an approximately sinusoidal function of ϕ_0 with maximum and minimum values near $\pi/2, 3\pi/2$, but these extreme points both move towards π with increasing Λ^* and the curve becomes multivalued with local maximum and minimum values of ϕ_0 for $\Lambda^* > \frac{1}{16}$.

If the rotation ϕ_0 of the fixed end of the rod is increased monotonically, a snap-through instability must occur from A to C, and a corresponding snap through from B to D must occur when ϕ_0 is decreased. However, instability could occur before these points if the system driving the fixed end of the rod has some finite stiffness, k . We define this stiffness such that a reaction torque T_0 applied to the drive system causes a local rotation

$$\beta = T_0/k. \tag{7.3}$$

Suppose we now keep the drive stationary while applying a small torque δT to the rod at $\theta = 0$. If the angle ϕ_0 increases to $\phi_0 + \Delta$, the torque in the rod will increase by $(dT_0/d\phi_0)\Delta$, while the reaction torque increases by $k\Delta$. The required increment of torque is therefore

$$\delta T = \left(k - \frac{dT_0}{d\phi_0} \right) \Delta \tag{7.4}$$

in the direction of the rotation Δ .

Normally, of course, a positive torque is required to achieve a positive rotation, but if

$$\frac{dT_0}{d\phi_0} > k, \tag{7.5}$$

the system will need restraining from further rotation after a small rotation from the equilibrium position and hence is unstable. This is clearly possible when the system

is in the regions EA and BF in figure 5 if the drive stiffness k is sufficiently low. If k is increased, the onset of instability will be moved towards the points A and B in figure 5. When condition (7.5) is satisfied, the rod will snap through to a new equilibrium position.

A special case of some interest is that in which there is a straight section of tube of length L between the (rigid) drive and the curved section. In this case, the rod itself constitutes a flexible drive for which

$$k = GK/L. \quad (7.6)$$

Thus, snap-through instabilities and significant rotational errors between input and output become more likely as L is increased. Notice that a straight section of tube at the free (non-driven) end has no such effect, since the rod in that section will be free of torque.

8. The non-axisymmetric rod

We now turn our attention to the case in which an initially straight rod ($\kappa_0 = \kappa'_0 = 0$) with different principal second moments of area I_1, I_2 is inserted into the plane circular channel of figure 2. Substituting these results into (4.2), (4.3), we find that the only non-zero function is

$$f_4 = \frac{1}{2}(E(I_1 - I_2)\rho_1^2), \quad (8.1)$$

and equation (4.7) reduces to

$$\frac{d^2\phi}{ds^2} = \frac{E(I_1 - I_2)}{2GK}\rho_1^2 \sin(2\phi) \quad (8.2)$$

or, in terms of the subtended angle θ ,

$$\frac{d^2\phi}{d\theta^2} = \frac{E(I_1 - I_2)}{2GK}\sin(2\phi). \quad (8.3)$$

This equation is clearly very similar to (6.6) and can in fact be reduced to that form by the change of variables

$$\phi = \frac{1}{2}\alpha, \quad \Lambda^* = \frac{E(I_1 - I_2)}{GK}. \quad (8.4)$$

The results of § 6 can therefore be carried over directly to the present problem.

The factor of 2 in the first of equations (8.4) implies that the figure analogous to figure 4 will be periodic in ϕ with period 180° instead of 360° , as we should expect, since the second moments of area of the section are periodic with period 180° . In physical terms, the initially curved axisymmetric rod has one minimum energy state, when the initial curvature is aligned with the curvature of the channel. By contrast, the non-axisymmetric rod has two such states, when the flexible principal axis is parallel to the positive or negative curvature axis Oy .

If the deviation from axisymmetry is small, we conclude from § 6*b* that the maximum error in ϕ_1 will occur when $\alpha_0 = \pi/2$ and, hence, $\phi_0 = \pi/4$. This is also the orientation that maximizes the product inertia of the rod cross-section in the channel coordinate system.

To find the maximum value, we adapt equation (6.18) using the relations from (8.4), obtaining

$$(\phi_0 - \phi_1)_{\max} = \frac{1}{2}(\alpha_0 - \alpha_1)_{\max} = \frac{1}{4}\theta_1^2 A^* = \frac{E(I_1 - I_2)\theta_1^2}{4GK}. \quad (8.5)$$

Thus, the maximum error depends on the square of the subtended angle θ_1 .

For an elliptical section of major and minor axes a , b , respectively,

$$I_1 = \frac{1}{4}\pi a^3 b, \quad I_2 = \frac{1}{4}\pi a b^3, \quad K = \frac{\pi a^3 b^3}{(a^2 + b^2)}, \quad (8.6)$$

from Timoshenko & Goodier (1970, § 105), and hence

$$(\phi_0 - \phi_1)_{\max} = \frac{(a^4 - b^4)(1 + \nu)\theta_1^2}{2a^2 b^2}, \quad (8.7)$$

using $E = 2G(1 + \nu)$. If this expression is not to exceed 0.01 rad and if $\theta_1 = 2\pi$, $\nu = 0.3$, we require

$$1 - \frac{b}{a} < 0.0001. \quad (8.8)$$

In other words, the circularity of the rod must be controlled to within 0.01%.

9. Conclusions

In this paper, we have developed an algorithm for using strain gauge measurements of local curvature of an endoscope biopsy channel to determine the location of the endoscope in the body. The rotational orientation ϕ of the probe cannot be measured, but it can be deduced by an updating algorithm as long as the rod on which the probe is mounted is axisymmetric and initially straight.

If the rod is not axisymmetric, the predicted value of ϕ will be in error by an angle that increases quadratically with the angle θ_1 subtended by the space curve of the channel. If the rod is axisymmetric but has some small initial curvature, the error is proportional to the product of the inserted length and the subtended angle. If the rod imperfections or the subtended angle are sufficiently large, snap-through instabilities can occur, rendering the proposed measurement method impractical.

The magnitude of the error is determined for the test case of insertion into a plane circular channel, and criteria are developed for determining the maximum permissible initial curvature or ratio of principal flexural rigidities. These criteria place quite stringent limits on the required straightness and symmetry of the rod for acceptable measurement accuracy.

F.V.K. and J.R.B. are pleased to acknowledge support from the National Science Foundation under contract no. CMS-9322106.

References

- Antman, S. S. 1974 Kirchhoff's problem for nonlinearly elastic rods. *Q. Appl. Math.* **32**, 221–240.
 Bladen, J. S., Anderson, A. P., Bell, G. D., Rameh, B., Evans, B. & Heatley, D. J. T. 1993 Non-radiological technique for three-dimensional imaging of endoscopes. *Lancet* **341**, 719–722.

- Hellinger, M. D. 1998 Screening and detection of colorectal cancer. *Cancer Control: JMCC* **5**, 17–18.
- Love, A. E. H. 1927 *A treatise on the mathematical theory of elasticity*, 4th edn. Cambridge University Press.
- Lu, C.-L. & Perkins, N. C. 1994 Nonlinear spatial equilibria and stability of cables under uniaxial torque and thrust. *ASME J. Appl. Mech.* **61**, 879–886.
- Nordgren, R. P. 1974 On computation of the motion of elastic rods. *ASME J. Appl. Mech.* **41**, 777–780.
- Rogers, B. H. G. 1990 Colonoscopy with fluoroscopy. *Gastrointest. Endosc.* **36**, 71–72.
- Shan, Y.-S. 1999 *Sensor device for spacial imaging of endoscopes*, US patent no. 5 957 833.
- Timoshenko, S. P. & Goodier, J. N. 1970 *Theory of elasticity*, 3rd edn. New York: McGraw-Hill.
- Williams, C., Guy, C., Gillies, D. & Saunders, B. 1993 Electronic three-dimensional imaging of intestinal endoscopy. *Lancet* **341**, 724–725.